Journal of Non-Newtonian Fluid Mechanics 327 (2024) 105216

Contents lists available at ScienceDirect

Journal of Non-Newtonian Fluid Mechanics

journal homepage: www.elsevier.com/locate/jnnfm

Full length article

The Gordon–Schowalter/Johnson–Segalman model in parallel and orthogonal superposition rheometry and its application in the study of worm-like micellular systems

A. Ogunkeye [a], R. Hudson-Kershaw [a], A.R. Davies [b], D.J. Curtis [a,*]

[a] Complex Fluids Research Group, Department of Chemical Engineering, School of Engineering and Applied Sciences, Faculty of Science and Engineering, Swansea University Bay Campus, Fabian Way, Swansea SA1 8EN, UK

[b] School of Mathematics, Cardiff University, Senghennydd Road, Cardiff CF24 4AG, UK

ARTICLE INFO

Keywords:
Superposition rheometry
Gordon–Schowalter model
Worm like micelles

ABSTRACT

Parallel and Orthogonal Superposition experiments may be employed to probe a material's non-linear rheological properties through the rate-dependent parallel and orthogonal superposition moduli, $G^*_{\parallel}(\omega,\dot{\gamma})$ and $G^*_{\perp}(\omega,\dot{\gamma})$, respectively. In a recent series of publications, we have considered the problem of interconversion between parallel and orthogonal superposition moduli as a means of probing flow induced anisotropy. However, as noted by Yamomoto (1971) superposition flows may be used to assess the ability of a particular constitutive model to describe the flow of complex fluids. Herein, we derive expressions for the superposition moduli of the Gordon–Schowalter (or Johnson–Segalman) fluid. This model contains, as special cases, the corotational Maxwell model, the upper (and lower) convected Maxwell models, the corotational Jeffreys model, and the Oldroyd-B model. We also consider the conditions under which the superposition moduli may take negative values before studying a specific, non shear banding, worm like micellular system of cetylpyridinium chloride and sodium salicylate. We find that, using a weakly non-linear analysis (in which the model parameters are rate independent) the Gordon–Schowalter/Johnson–Segalman (GS/JS) model is unable to describe the superposition moduli. However, by permitting strong non-linearity (allowing the GS/JS parameters to become shear rate dependent), the superposition moduli, at all rates studied, are described well by the model. Based on this strongly non-linear analysis, the shear rate dependency of the GS/JS 'slip parameter', a, suggests that the onset of shear thinning in the specific worm-like micellular system studied herein is driven by a combination of microstructural modification and a transition from rotation dominated (as in the corotational Jeffreys model) to shear dominated (as in the Oldroyd-B model) deformation of the microstructural elements.

1. Introduction

Superposition Rheometry may be used to characterise the non-linear rheological properties of complex fluids. The techniques involve the simultaneous application of (i) a unidirectional shear flow that drives the fluid into a steady, but non-equilibrium, condition and (ii) a small amplitude oscillatory flow that probes the frequency-dependent rheological characteristics of the material at the imposed unidirectional shear rate. The oscillatory component may be applied in either a 'parallel' (PSR) or 'orthogonal' (OSR) configuration. In PSR, the unidirectional and oscillatory flow components are applied in the same direction whilst in OSR the oscillatory component is applied orthogonally to the unidirectional flow. Analysis of the oscillatory flow component allows one to report the frequency and strain-rate dependent parallel or orthogonal superposition complex moduli, $G^*_{\parallel}(\omega,\dot{\gamma})$ and $G^*_{\perp}(\omega,\dot{\gamma})$, respectively. Whilst it is tempting to interpret these parameters as per the linear modulus, $G^*(\omega)$ it is important to note that their relationship to the underlying stress relaxation characteristics of the fluid are not the same as those of $G^*(\omega)$ [1–5].

The techniques of Superposition Rheometry were first discussed in the literature in the 1960's [1,6–9]. Until very recently, the orthogonal experiment could only be performed using a TA Instruments ARES-G2 rheometer fitted with specialist geometries [2,10] (or using bespoke instrumentation/rheometer adaptations [11–14]). Consequently, experimental studies employing orthogonal superposition are scarce. However, in the past few years, orthogonal superposition accessories have become available for a wider range of rheometers including the HR series from TA Instruments and the MCR series of rheometers from Anton-Paar (as a bespoke accessory). In contrast, the PSR experiment can be implemented on most single head rheometers using

* Corresponding author.
E-mail address: d.j.curtis@swansea.ac.uk (D.J. Curtis).

https://doi.org/10.1016/j.jnnfm.2024.105216
Received 15 January 2024; Received in revised form 6 March 2024; Accepted 7 March 2024
Available online 14 March 2024

standard geometries. However, the complexity of the expressions relating the parallel moduli to the underlying relaxation characteristics of the material, such as those derived by Yamamoto [1] for a Lodge type integral constitutive model (lodge 'type' because the underlying relaxation spectrum was allowed to be shear-rate dependent — thus permitting strong non-linearity) led to a widespread belief that the parallel moduli were not Kramers–Krönig (KK) compliant. However, whilst considering the problem of interconversion between the parallel and orthogonal complex moduli, Curtis & Davies [3] approached the analysis of the Lodge style integral constitutive model of Yamamoto in terms of a rate-dependent response spectrum and demonstrated that both parallel and orthogonal moduli are indeed, KK compliant. The same authors have also derived expressions for the superposition moduli for the Wagner-I and K-BKZ [4], and corotational Maxwell [5] (CRM) models, demonstrating that the superposition moduli for these models are also KK compliant.

Closely related to the CRM, the Gordon–Schowalter (GS) [15] model (which is equivalent to the Johnson–Segalman (JS) model [16] in the limit of the single mode [17]) is a differential model derived by introducing the GS convected derivative (see Section 2.2), in contrast, the JS model is an integral model derived by admitting a non-affine velocity gradient to the Lodge integral constitutive equation. As discussed by Ramlawi et al. [17] in their study of the weakly nonlinear response of the JS model, the latter is more general and, in contrast to the GS model (which was derived for polymeric materials), is not restricted to a particular microstructure. The terms GS and JS appear to be used interchangeably in the literature. In the present work, we limit our discussion to a single mode and hence refer to the GS/JS model throughout. The GS/JS model contains a 'slip' or 'affinity' parameter, a, which permits the polymer chains and the bulk solvent to experience different velocity gradients - i.e. the polymer chains 'slip' relative to the velocity gradient imposed by the bulk deformation. Where $a = 0$ the GS/JS model reduces to the corotational Maxwell (CRM) model, whilst for $a = 1$ the model reduces to the Upper Convected Maxwell (UCM) model. Herein, we derive expressions for the parallel and orthogonal superposition moduli of the GS/JS model which may be used to facilitate model based interconversion between the superposition moduli to support the study of flow induced anisotropy (as discussed in [5]). However, the techniques of superposition rheometry are also excellent tools for assessing the ability of constitutive models to describe particular fluids [1].

In the present work, we assess the ability of the CRM and GS/JS constitutive models to describe the dynamics of a (non shear-banding) Worm-like Micellular (WLM) system (cetylpyridinium chloride/sodium salicylate) under superposition flows where the analysis has been performed on (i) a weakly non-linear and (ii) a strongly non-linear basis. In defining these conditions we draw on the definitions provided by Malkin (1995) [18] who proposed that flows should be considered weakly non-linear where the underlying relaxation spectrum is not modified by the flow but strongly non-linear where the materials microstructural response to the imposed flow condition generates changes to its underlying relaxation properties - i.e. in the strongly non-linear regime the flow shear stresses can no longer be predicted from the linear relaxation spectrum (in combination with some non-linear parameter) and, in terms of superposition rheometry, leads to rate-dependent parameterisation of the flow models.

Many constitutive models have been proposed, and used, to study WLM systems [19–21]. Anderson, Pearson & Sherwood (2006) [22] evaluated the ability of the Bautista-Monero and a Modified-Bautista–Monero constitutive models to capture the dynamics of a WLM system under parallel superposition flows concluding that neither model performed well and noting that 'often rheological models that are in excellent agreement with a restricted set of experimental results perform poorly when used to predict flows other than those on which they have been calibrated' [22]. Ballesta et al. [23] studied shear banding WLM using parallel superposition using a two-fluid model. As part of their treatment they employed the Oldroyd-B model for which Booij (1966) [24] derived expressions for the superposition moduli. Kim et al. (2013) [2] derived approximate solutions for the superposition moduli (both parallel and orthogonal) for the Giesekus model and found the model was able to capture some features of the experimental data for a shear thinning WLM system but was unable to predict the superposition moduli under shear banding conditions. Recently, Medium-Amplitude-Parallel-Superposition (MAPS) rheometry (which includes the parallel superposition experiment as a special case) on a WLM system has been reported by Lennon et al. [25] who demonstrated that the CRM was able to better describe the high frequency dynamics of a WLM system than the Giesekus model. The authors also noted that the use of constitutive models specifically formulated for WLM systems would give better insight into the physical processes that underlie the rheological data. In the present work, we also adopt a relatively simple constitutive modelling approach (using the CRM and JS/GS models) with a view to exploring microstructure based constitutive models in future work. For example, whilst the JS/GS model has been used to study shear banding, its successful implementation requires the inclusion of a stress diffusion term which we leave to further work [26,27]. The remainder of this article begins by reviewing the expressions for the superposition moduli for the corotational Maxwell model (as derived in [5]) before extending the analysis to the GS/JS model (incorporating the 'slip' parameter 'a'). We then present experimental data for a specific (non-shear banding) worm-like micellular system (cetylpyridinium chloride/sodium salicylate/sodium chloride) before analysing the data in the context of both (i) weak and (ii) strong non-linearity using the corotational Jeffreys model (i.e. the CRM with a Newtonian solvent) and GS/JS models (with Newtonian solvent).

2. Modelling

In [5], Curtis & Davies derived expressions for the parallel and orthogonal superposition moduli for the corotational Maxwell model. The reader is referred to Ref. [5] for details of the derivation but the main results are provided below for convenience.

2.1. Corotational Maxwell model

We begin by writing the Cauchy stress tensor as:

$$\boldsymbol{\sigma} = -p\mathbf{I} + \boldsymbol{\tau} \tag{2.1}$$

for which the extra stress tensor $\boldsymbol{\tau}$ can be written as:

$$\boldsymbol{\tau} + \lambda \frac{D\boldsymbol{\tau}}{Dt} = \eta_0 \dot{\boldsymbol{\gamma}} \tag{2.2}$$

For the corotational Maxwell model, the objective derivative is the corotational, or Jaumann, derivative defined as:

$$\frac{D\boldsymbol{\tau}}{Dt} = \frac{D\boldsymbol{\tau}}{Dt} + \frac{1}{2}\left[\boldsymbol{\omega}\cdot\boldsymbol{\tau} - \boldsymbol{\tau}\cdot\boldsymbol{\omega}\right] \tag{2.3}$$

For a parallel superposition flow, with arbitrary superimposed perturbation $\epsilon\dot{\phi}(t)$ (e.g. oscillation, step, chirp) to the viscometric flow (characterised by a steady, unidirectional, shear rate $\dot{\gamma}$) we can write the velocity field as:

$$\boldsymbol{u}_{\parallel} = \left[(\dot{\gamma} + \epsilon\dot{\phi})y, 0, 0\right]^T \tag{2.4}$$

whilst for an orthogonal experiment we can write

$$\boldsymbol{u}_{\perp} = \left[\dot{\gamma}y, 0, \epsilon\dot{\phi}y\right]^T \tag{2.5}$$

In the present work we restrict or attention to simple (i.e. single tone) oscillatory perturbations and hence $\phi(t) = e^{-i\omega t}$. For later use, we define the vorticity and strain rate tensors as:

$$\boldsymbol{\omega} = \nabla\boldsymbol{u} - \nabla\boldsymbol{u}^T \tag{2.6}$$

and

$$\dot{\boldsymbol{\gamma}} = \nabla\boldsymbol{u} + \nabla\boldsymbol{u}^T \tag{2.7}$$

For such flows, the material derivative in (2.3) (i.e. $D\tau/Dt$) reduces to the normal derivative (i.e. $d\tau/dt$). Using a power series expansion about the viscometric flow case we can write the following expressions for the parallel and orthogonal moduli [5]:

$$G'_{\parallel}(\dot{\gamma},\omega) = \frac{\eta_0\omega^2\lambda_1(1+\omega^2\lambda_1^2-3\lambda_1^2\dot{\gamma}^2)}{(1+\lambda_1^2\dot{\gamma}^2)[(1+\lambda_1^2\dot{\gamma}^2-\omega^2\lambda_1^2)^2+4\omega^2\lambda_1^2]} \tag{2.8}$$

$$G''_{\parallel}(\dot{\gamma},\omega) = \frac{\eta_0\omega(1+\omega^2\lambda_1^2-\lambda_1^2\dot{\gamma}^2)}{(1+\lambda_1^2\dot{\gamma}^2-\omega^2\lambda_1^2)^2+4\omega^2\lambda_1^2} \tag{2.9}$$

$$G'_{\perp}(\dot{\gamma},\omega) = \frac{\eta_0\omega^2\lambda_1}{1+\lambda_1^2\dot{\gamma}^2}\left[\frac{\left(1+\frac{1}{2}\lambda_1^2\dot{\gamma}^2\right)\omega^2\lambda_1^2+\left(1+\frac{1}{4}\lambda_1^2\dot{\gamma}^2\right)\left(1-\frac{1}{2}\lambda_1^2\dot{\gamma}^2\right)}{(1+\frac{1}{4}\lambda_1^2\dot{\gamma}^2-\omega^2\lambda_1^2)^2+4\omega^2\lambda_1^2}\right] \tag{2.10}$$

$$G''_{\perp}(\dot{\gamma},\omega) = \frac{\eta_0\omega}{1+\lambda_1^2\dot{\gamma}^2}\left[\frac{\left(1+\frac{1}{4}\lambda_1^2\dot{\gamma}^2\right)^2+\omega^2\lambda_1^2\left(1+\frac{3}{4}\lambda_1^2\dot{\gamma}^2\right)}{(1+\frac{1}{4}\lambda_1^2\dot{\gamma}^2-\omega^2\lambda_1^2)^2+4\omega^2\lambda_1^2}\right] \tag{2.11}$$

2.2. Parallel superposition moduli for the Gordon–Schowalter/Johnson–Segalman model

The GS/JS Model [15,16], includes a parameter, $-1 \le a \le 1$, interpreted as a 'slip parameter' that allows the polymer (or other microstructural element) to experience non-affine deformation. The model contains the upper convected, lower convected and corotational Maxwell models as special cases (corresponding to $a = -1, 1$ and 0, respectively). As for the CRM, to derive expressions for the superposition moduli we begin by writing the Cauchy stress tensor as:

$$\boldsymbol{\sigma} = -p\mathbf{I} + \boldsymbol{\tau} \tag{2.12}$$

for which the extra stress tensor $\boldsymbol{\tau}$ can be written as:

$$\boldsymbol{\tau} + \lambda\frac{\mathcal{D}\boldsymbol{\tau}}{\mathcal{D}t} = \eta_0\dot{\boldsymbol{\gamma}} \tag{2.13}$$

where the objective derivative is the Gordon–Schowalter [15] derivative defined as:

$$\frac{\mathcal{D}\boldsymbol{\tau}}{\mathcal{D}t} = \frac{D\boldsymbol{\tau}}{Dt} + \frac{1}{2}\left[(\boldsymbol{\omega}-a\dot{\boldsymbol{\gamma}})\cdot\boldsymbol{\tau}-\boldsymbol{\tau}\cdot(\boldsymbol{\omega}+a\dot{\boldsymbol{\gamma}})\right] \tag{2.14}$$

However, for superposition flows, the material derivative in (2.14) reduces to the normal derivative such that

$$\frac{\mathcal{D}\boldsymbol{\tau}}{\mathcal{D}t} = \frac{d\boldsymbol{\tau}}{dt} + \frac{1}{2}\left[(\boldsymbol{\omega}-a\dot{\boldsymbol{\gamma}})\cdot\boldsymbol{\tau}-\boldsymbol{\tau}\cdot(\boldsymbol{\omega}+a\dot{\boldsymbol{\gamma}})\right] \tag{2.15}$$

The extra stress tensor, $\boldsymbol{\tau}$ is symmetric and may be written as six component equations. For the parallel superposition case, (where the velocity field is defined by Eq. (2.4)) the constraint $\tau_{13} = \tau_{23} = \tau_{33} = 0$ is admitted and the following set of linear differential equations in τ_{11}, τ_{22} and τ_{12} may be written:

$$\tau_{11} + \lambda_1\left[\dot{\tau}_{11} - (\dot{\gamma}+\epsilon\dot{\phi}(t))\tau_{21}(1+a)\right] = 0 \tag{2.16}$$

$$\tau_{12} + \lambda_1\dot{\tau}_{12} + \frac{\lambda_1}{2}(\dot{\gamma}+\epsilon\dot{\phi}(t))\left[(1-a)\tau_{11}-(1+a)\tau_{22}\right] = \eta_0(\dot{\gamma}+\epsilon\dot{\phi}(t)) \tag{2.17}$$

$$\tau_{22} + \lambda_1\left[\dot{\tau}_{22} + (\dot{\gamma}+\epsilon\dot{\phi}(t))\tau_{21}(1-a)\right] = 0 \tag{2.18}$$

Further, from Eqs. (2.16) and (2.18) we can write,

$$\tau_{22} = -\left(\frac{1-a}{1+a}\right)\tau_{11} \tag{2.19}$$

which allows us to write the following pair of linear differential equations:

$$\tau_{11} + \lambda_1\dot{\tau}_{11} - \lambda_1\dot{\gamma}(1+a)\tau_{21} - \epsilon\lambda_1\dot{\phi}(t)\tau_{21}(1+a) = 0 \tag{2.20}$$

$$\tau_{12} + \lambda_1\dot{\tau}_{12} + \lambda_1(1-a)\dot{\gamma}\tau_{11} + \epsilon\lambda_1(1-a)\dot{\phi}(t)\tau_{11} = \eta_0\dot{\gamma} + \epsilon\eta_0\dot{\phi}(t) \tag{2.21}$$

Considering the viscometric case, i.e. $\epsilon = 0$, Eqs. (2.20) and (2.21) reduce to:

$$\tau_{11} - \lambda_1\dot{\gamma}(1+a)\tau_{21} = 0 \tag{2.22}$$

$$\tau_{12} + \lambda_1(1-a)\dot{\gamma}\tau_{11} = \eta_0\dot{\gamma} \tag{2.23}$$

from which we can write the viscometric expressions for τ_{11} and τ_{12} as:

$$\tau_{11}^{(0)} = \frac{\eta_0\lambda_1\dot{\gamma}^2(1+a)}{1+\lambda_1^2\dot{\gamma}^2(1-a^2)} \tag{2.24}$$

and

$$\tau_{12}^{(0)} = \frac{\eta_0\dot{\gamma}}{1+\lambda_1^2\dot{\gamma}^2(1-a^2)} \tag{2.25}$$

which, for $a = 0$, reduce the expressions for the corotational Maxwell model as expected.

We now represent the extra stress tensor as a power series:

$$\boldsymbol{\tau} = \boldsymbol{\tau}^{(0)}(t) + \epsilon\boldsymbol{\tau}^{(1)}(t) + \epsilon^2\boldsymbol{\tau}^{(2)}(t) + \cdots \tag{2.26}$$

and substitute into Eqs. (2.20) and (2.21) to give:

$$[\tau_{11}^{(0)}+\epsilon\tau_{11}^{(1)}] + \lambda_1[\dot{\tau}_{11}^{(0)}+\epsilon\dot{\tau}_{11}^{(1)}] - \lambda_1\dot{\gamma}(1+a)[\tau_{12}^{(0)}+\epsilon\tau_{12}^{(1)}] - \epsilon\lambda_1\dot{\phi}(t)[\tau_{12}^{(0)}+\epsilon\tau_{12}^{(1)}](1+a) = 0 \tag{2.27}$$

$$[\tau_{12}^{(0)}+\epsilon\tau_{12}^{(1)}] + \lambda_1[\dot{\tau}_{12}^{(0)}+\epsilon\dot{\tau}_{12}^{(1)}] + \lambda_1(1-a)\dot{\gamma}[\tau_{11}^{(0)} + \epsilon\tau_{11}^{(1)}] + \epsilon\lambda_1(1-a)\dot{\phi}(t)[\tau_{11}^{(0)}+\epsilon\tau_{11}^{(1)}] = \eta_0\dot{\gamma} + \epsilon\eta_0\dot{\phi}(t) \tag{2.28}$$

Noting that $\dot{\tau}_{11}^{(0)} = \dot{\tau}_{12}^{(0)} = 0$ and substituting Eqs. (2.24) and (2.25) for $\tau_{11}^{(0)}$ and $\tau_{12}^{(0)}$, respectively we can write (to first order in ϵ):

$$\tau_{11}^{(1)} + \lambda_1\dot{\tau}_{11}^{(1)} - \lambda_1\dot{\gamma}(1+a)\tau_{12}^{(1)} = \alpha\dot{\phi}(t) \tag{2.29}$$

$$\tau_{12}^{(1)} + \lambda_1\dot{\tau}_{12}^{(1)} + \lambda\dot{\gamma}(1-a)\tau_{11}^{(1)} = \beta\dot{\phi}(t) \tag{2.30}$$

where

$$\alpha = \frac{\eta_0\lambda_1\dot{\gamma}(1+a)}{1+\lambda_1^2\dot{\gamma}^2(1-a^2)} \tag{2.31}$$

$$\beta = \frac{\eta_0}{1+\lambda_1^2\dot{\gamma}^2(1-a^2)} \tag{2.32}$$

Note that β is equal to the rate-dependent viscosity for the viscoemetric case (see Eq. (2.25)).

For a parallel superposition experiment with a single tone sinusoidal perturbation (i.e. a standard PSR experiment), the first order shear stress may be written in the form:

$$\tau_{12}^{(1)}(t) = G_{\parallel}^*(\dot{\gamma},\omega)e^{i\omega t} \tag{2.33}$$

where $G_{\parallel}^*(\dot{\gamma},\omega)$ denotes the usual rate-dependent parallel superposition complex modulus. Writing $\phi(t) = e^{i\omega t}$ in Eqs. (2.29) and (2.30), it is also clear that $\tau_{11}^{(1)}$ will take the form:

$$\tau_{11}^{(1)}(t) = A(\omega)e^{i\omega t} \tag{2.34}$$

Hence, we can write Eqs. (2.29) and (2.30) as:

$$A(\dot{\gamma},\omega)(1+\lambda_1 i\omega) - \lambda_1\dot{\gamma}(1+a)G_{\parallel}^*(\dot{\gamma},\omega) = \alpha i\omega \tag{2.35}$$

$$G_{\parallel}^*(\dot{\gamma},\omega)(1+\lambda_1 i\omega) + \lambda_1\dot{\gamma}(1-a)A(\dot{\gamma},\omega) = \beta i\omega \tag{2.36}$$

Solving for $G_{\parallel}^*(\dot{\gamma},\omega)$, we find:

$$G_{\parallel}^*(\dot{\gamma},\omega) = \frac{\eta_0 i\omega}{1+\lambda_1^2\dot{\gamma}^2(1-a^2)}\left[\frac{(1+\lambda_1 i\omega)-\lambda_1^2\dot{\gamma}^2(1-a^2)}{(1+\lambda_1 i\omega)^2+\lambda_1^2\dot{\gamma}^2(1-a^2)}\right] \tag{2.37}$$

which reduces to (i) the expression for the corotational Maxwell model when $a = 0$ and (ii) the linear viscoelastic modulus when $\dot{\gamma} = 0$.

Resolving Eq. (2.37) into its real and imaginary parts, we arrive at the expressions for the parallel storage and loss moduli, respectively.

$$G'_{\parallel}(\dot{\gamma},\omega) = \frac{\eta_0\omega^2\lambda_1(1+\omega^2\lambda_1^2-3\lambda_1^2\dot{\gamma}^2(1-a^2))}{(1+\lambda_1^2\dot{\gamma}^2(1-a^2))[(1+\lambda_1^2\dot{\gamma}^2(1-a^2)-\omega^2\lambda_1^2)^2+4\omega^2\lambda_1^2]} \tag{2.38}$$

$$G''_{\parallel}(\dot{\gamma},\omega) = \frac{\eta_0\omega(1+\omega^2\lambda_1^2-\lambda_1^2\dot{\gamma}^2(1-a^2))}{(1+\lambda_1^2\dot{\gamma}^2(1-a^2)-\omega^2\lambda_1^2)^2+4\omega^2\lambda_1^2} \tag{2.39}$$

It is instructive to consider the conditions for which negative values of the parallel moduli may appear. Noting that $\lambda_1 > 0$, $\omega > 0$ and $-1 \le a \le 1$ we can see that:

1. The condition for $G'_{\parallel}(\dot{\gamma},\omega)$ to be globally positive (i.e. $G'_{\parallel}(\dot{\gamma},\omega) > 0$ for all positive ω) is that

   $\lambda_1^2\dot{\gamma}^2(1-a^2) < \frac{1}{3}$.

   Otherwise, $G'_{\parallel}(\dot{\gamma},\omega) < 0$ where

   $\omega^2\lambda_1^2 < 3\lambda_1^2\dot{\gamma}^2(1-a^2) - 1$.

2. The condition for $G''_{\parallel}(\dot{\gamma},\omega)$ to be globally positive is that

   $\lambda_1^2\dot{\gamma}^2(1-a^2) < 1$.

   Otherwise, $G''_{\parallel}(\dot{\gamma},\omega) < 0$ where

   $\omega^2\lambda_1^2 < \lambda_1^2\dot{\gamma}^2(1-a^2) - 1$.

Hence, for a given frequency, $G'_{\parallel}(\dot{\gamma},\omega)$ will become negative at lower $\dot{\gamma}$ than $G''_{\parallel}(\dot{\gamma},\omega)$.

The frequency at which the moduli change sign ($\omega'_{c\parallel}$ and $\omega''_{c\parallel}$ for $G'_{\parallel}(\dot{\gamma},\omega)$ and $G''_{\parallel}(\dot{\gamma},\omega)$, respectively) can be written as:

$$\omega'_{c\parallel} = \sqrt{3\dot{\gamma}^2(1-a^2) - \frac{1}{\lambda_1^2}} \tag{2.40}$$

and

$$\omega''_{c\parallel} = \sqrt{\dot{\gamma}^2(1-a^2) - \frac{1}{\lambda_1^2}} \tag{2.41}$$

from which we see that, provided the criteria for globally positive moduli are not met, for a given shear rate and relaxation time, increasing $|a|$ pushes both $\omega'_{c\parallel}$ and $\omega''_{c\parallel}$ to lower values with $\omega'_{c\parallel} > \omega''_{c\parallel}$ until, at

$$|a| = \sqrt{1 - \frac{1}{\lambda_1^2\dot{\gamma}^2}}$$

$\omega''_{c\parallel}$ reaches zero and globally positive $G''_{\parallel}(\dot{\gamma},\omega)$ are recovered before, at

$$|a| = \sqrt{1 - \frac{1}{3\lambda_1^2\dot{\gamma}^2}}$$

$\omega'_{c\parallel}$ reaches zero and globally positive $G'_{\parallel}(\dot{\gamma},\omega)$ are recovered.

2.2.1. Kramers–Krönig compliance of the GS/JS parallel moduli

As noted in Section 1, it is often claimed in the literature that the parallel superposition moduli do not satisfy the Kramers–Krönig relations. This assertion appears to be based on the seminal work of Yamamoto (1973) [1] in which he derived expressions for $G'_{\parallel}(\dot{\gamma},\omega)$ and $G''_{\parallel}(\dot{\gamma},\omega)$ for a Lodge-type integral constitutive equation (specifically 'Lodge-type' because Yamamoto allowed the memory function of the Lodge model to become shear rate dependent). Yamamoto's expressions were believed to invalidate the Kramers–Krönig relations for over 4 decades but it has recently been shown that the expressions could be rewritten as a pair of Kramers–Krönig compliant moduli. Since then, the K-BKZ and Wagner I models [4], and the CRM model [5] have also been shown to have Kramers–Krönig compliant parallel (and orthogonal) moduli. The parallel moduli for the GS/JS model (Eqs. (2.38) and (2.39)) also satisfy the Kramers–Krönig relations since $G^*_{\parallel}(\dot{\gamma},\omega)$, apart from at its poles (which occur, in the upper half of the complex frequency plane, at $\omega = \pm\dot{\gamma}\sqrt{(1-a^2)} + i\lambda_1^{-1}$), is an analytic function of ω throughout the complex frequency plane.

2.3. Orthogonal superposition for the Gordon-Schowalter model

For orthogonal superposition experiments, in which the flow field is defined by Eq. (2.5), expansion of the extra stress tensor around the viscometric case (see Appendix) leads to a set of six linear simultaneous differential equations. Of these, the τ_{13} and τ_{23} components define a solvable pair from which the orthogonal moduli can be determined:

$$\tau_{13}^{(1)} + \lambda_1\dot{\tau}_{13}^{(1)} - \frac{1}{2}\lambda_1\dot{\gamma}(1+a)\tau_{23}^{(1)} = \frac{1}{2}\alpha\dot{\phi} \tag{2.42}$$

$$\tau_{23}^{(1)} + \lambda_1\dot{\tau}_{23}^{(1)} + \frac{\lambda_1}{2}\dot{\gamma}(1-a)\tau_{13}^{(1)} = \frac{1}{2}(\beta+\eta_0)\dot{\phi} \tag{2.43}$$

For an orthogonal superposition experiment with a single tone sinusoidal perturbation, the first order orthogonal shear stress (τ_{23}) can be written

$$\tau_{23}^{(1)}(t) = G^*_{\perp}(\dot{\gamma},\omega)e^{i\omega t} \tag{2.44}$$

where $G^*_{\perp}(\dot{\gamma},\omega)$ denotes the usual rate-dependent orthogonal superposition complex modulus. Writing $\phi(t) = e^{i\omega t}$ in Eqs. (2.42) and (2.43), it is also clear that $\tau_{23}^{(1)}$ will take the form:

$$\tau_{13}^{(1)}(t) = B(\dot{\gamma},\omega)e^{i\omega t} \tag{2.45}$$

Hence, Eqs. (2.42) and (2.43) can be written as:

$$B(\dot{\gamma},\omega) + \lambda_1 i\omega B(\dot{\gamma},\omega) - \frac{1}{2}\lambda_1\dot{\gamma}(1+a)G^*_{\perp}(\dot{\gamma},\omega) = \frac{1}{2}\alpha i\omega \tag{2.46}$$

$$G^*_{\perp}(\dot{\gamma},\omega) + \lambda_1 i\omega G^*_{\perp}(\dot{\gamma},\omega) + \frac{\lambda_1}{2}\dot{\gamma}(1-a)B(\dot{\gamma},\omega) = \frac{1}{2}(\beta+\eta_0)i\omega \tag{2.47}$$

Solving for $G^*_{\perp}(\dot{\gamma},\omega)$ we find:

$$G^*_{\perp}(\dot{\gamma},\omega) = \frac{\eta_0 i\omega}{1+\lambda_1^2\dot{\gamma}^2(1-a^2)}\left[\frac{(1+i\omega\lambda_1)+\frac{1}{4}\lambda_1^2\dot{\gamma}^2(1-a^2)(1+2i\omega\lambda_1)}{(1+i\omega\lambda_1)^2+\frac{1}{4}\lambda_2\dot{\gamma}^2(1-a^2)}\right] \tag{2.48}$$

which can be resolved into its real and imaginary parts to find $G'_{\perp}(\dot{\gamma},\omega)$ and $G''_{\perp}(\dot{\gamma},\omega)$, respectively:

$$G'_{\perp}(\dot{\gamma},\omega) = \frac{\eta_0\omega^2\lambda_1}{1+\lambda_1^2\dot{\gamma}^2(1-a^2)} \times \left[\frac{(1+\frac{1}{2}\lambda_1^2\dot{\gamma}^2(1-a^2))\omega^2\lambda_1^2+(1+\frac{1}{4}\lambda_1^2\dot{\gamma}^2(1-a^2))(1-\frac{1}{2}\lambda_1^2\dot{\gamma}^2(1-a^2))}{(1+\frac{1}{4}\lambda_1^2\dot{\gamma}^2(1-a^2)-\omega^2\lambda_1^2)^2+4\omega^2\lambda_1^2}\right] \tag{2.49}$$

$$G''_{\perp}(\dot{\gamma},\omega) = \frac{\eta_0\omega}{1+\lambda_1^2\dot{\gamma}^2(1-a^2)} \times \left[\frac{(1+\frac{1}{4}\lambda_1^2\dot{\gamma}^2(1-a^2))^2+\omega^2\lambda_1^2(1+\frac{3}{4}\lambda_1^2\dot{\gamma}^2(1-a^2))}{(1+\frac{1}{4}\lambda_1^2\dot{\gamma}^2(1-a^2)-\omega^2\lambda_1^2)^2+4\omega^2\lambda_1^2}\right] \tag{2.50}$$

It is again interesting to note the conditions for which negative values of the moduli may appear. Noting that $\lambda_1 > 0$, $\omega > 0$ and $-1 \le a \le 1$ we see that:

1. The condition for $G'_{\perp}(\dot{\gamma},\omega)$ to be globally positive (i.e. $G'_{\perp}(\dot{\gamma},\omega) > 0$ for all positive ω) is that

   $\lambda_1^2\dot{\gamma}^2(1-a^2) < 2$

   Otherwise, $G'_{\perp}(\dot{\gamma},\omega) < 0$ where

   $$\omega^2\lambda_1^2 < \frac{(1+\frac{1}{4}\lambda_1^2\dot{\gamma}^2(1-a^2))(\lambda_1^2\dot{\gamma}^2(1-a^2)-2)}{2+\lambda_1^2\dot{\gamma}^2(1-a^2)}$$

2. $G''_{\perp}(\dot{\gamma},\omega)$ is always globally positive

Where $\lambda_1^2\dot{\gamma}^2(1-a^2) < 2$, the frequency at which $G'_{\perp}(\dot{\gamma},\omega)$ changes sign ($\omega'_{c\perp}$) can be written as:

$$\omega'_{c\perp} = \frac{(1+\frac{1}{4}\lambda_1^2\dot{\gamma}^2(1-a^2))(\lambda_1^2\dot{\gamma}^2(1-a^2)-2)}{\lambda_1^2(2+\lambda_1^2\dot{\gamma}^2(1-a^2))}$$

from which we see that, for a given shear rate and relaxation time, increasing $|a|$ again pushes ω'_c to lower values until, at

$$|a| = \sqrt{1-\frac{2}{\lambda_1^2\dot{\gamma}^2}}$$

ω'_c reaches zero and globally positive $G'_{\perp}(\dot{\gamma},\omega)$ is recovered.

2.4. The upper and lower convected Maxwell fluids

For $a = 1$ and $a = -1$, the GS model reduces to the upper and lower convected Maxwell models, respectively (UCM & LCM). In both of these limits, the expressions for the superposition moduli are:

$$G'_{\parallel}(\dot{\gamma},\omega) = G'_{\perp}(\dot{\gamma},\omega) = G'(\omega) = \frac{\eta_0\lambda_1\omega^2}{1+\omega^2\lambda_1^2} \tag{2.51}$$

$$G''_{\parallel}(\dot{\gamma},\omega) = G''_{\perp}(\dot{\gamma},\omega) = G''(\omega) = \frac{\eta_0\omega}{1+\omega^2\lambda_1^2} \tag{2.52}$$

We see that for both the UCM and LCM models, the superposition moduli in parallel and orthogonal experiments reduce to the linear moduli such that their shear rate dependency (and hence the possibility of negative values of the superposition moduli) are lost. This result is unsurprising since the UCM and LCM models do not display shear thinning in the viscometric case. We conjecture (in the absence of any evidence to the contrary) that shear thinning is required for the emergence of negative moduli (i.e. shear thinning is necessary, but not sufficient, since the real and imaginary parts of both sets of superposition moduli for the GS/JS model are globally positive for $\lambda_1^2\dot{\gamma}^2(1-a^2) < \frac{1}{3}$).

2.5. Comparison of the models

Fig. 1 shows parallel and orthogonal moduli as a function of Deborah number ($De = \lambda_1\omega$) at an indicative Weissenberg number ($Wi = \lambda_1\dot{\gamma}$) of 1.0 for a single mode GS/JS model for values of $|a|$ in the range $0.0 \le |a| \le 1.0$. There are several interesting features of these plots, (i) the parallel moduli are far more sensitive to the value of a than the orthogonal moduli, (ii) for $De \approx 2.0$ and above, $G''_{\parallel}$ is almost independent of the value of $|a|$ whilst $G'_{\parallel}$ increases with $|a|$.

2.6. Newtonian solvents

In the presence of a Newtonian solvent, with viscosity η_1, both $G^*_{\parallel}(\omega,\dot{\gamma})$ and $G^*_{\perp}(\omega,\dot{\gamma})$ for the CRM and GS models to carry the additional term $i\omega\eta_1$ [5]. Hence,

$$G''_{\parallel}(\dot{\gamma},\omega) = \frac{\eta_0\omega(1+\omega^2\lambda_1^2-\lambda_1^2\dot{\gamma}^2(1-a^2))}{(1+\lambda_1^2\dot{\gamma}^2(1-a^2)-\omega^2\lambda_1^2)^2+4\omega^2\lambda_1^2} + \eta_1\omega \tag{2.53}$$

and

$$G''_{\perp}(\dot{\gamma},\omega) = \frac{\eta_0\omega}{1+\lambda_1^2\dot{\gamma}^2(1-a^2)} \times \left[\frac{(1+\frac{1}{4}\lambda_1^2\dot{\gamma}^2(1-a^2))^2+\omega^2\lambda_1^2(1+\frac{3}{4}\lambda_1^2\dot{\gamma}^2(1-a^2))}{(1+\frac{1}{4}\lambda_1^2\dot{\gamma}^2(1-a^2)-\omega^2\lambda_1^2)^2+4\omega^2\lambda_1^2}\right] + \eta_1\omega \tag{2.54}$$

In the limits $a = 0$ and $a = 1$, in the presence of a Newtonian solvent, the CRM and UCM models may be referred to as the co-rotational Jeffreys model (CRJ) and the Oldroyd-B fluid, respectively.

3. Experimental methods

3.1. Materials

A 4.1 wt% cetylpyridinium chloride (CPyCl) and sodium salicylate (NaSal) (Sigma-Aldrich) were dissolved at a molar ratio of 2:1 in 0.5 M sodium chloride (NaCl) solutions prepared using deionised H_2O. Appropriate quantities of dry of NaCl, NaSal and CPyCl, in powdered form, were added to H_2O in a fume hood. The mixtures were stirred for 24 h at 40 °C (in a sealed beaker atop a heated plate) to completely disperse the powder before measurements were performed. All chemicals were used as received without further purification. At a concentration of 4.1 wt% CpyCl this formulation has been reported to display shear thinning characteristics in contrast to higher concentrations which have been shown to exhibit shear banding characteristics [28–30]. In the present work we restrict our attention to 'non-shear banding' formulations.

3.2. Rheometry

Rheological measurements were performed on a TA Instruments ARES-G2 rheometer adapted to permit orthogonal superposition experiments. The instrument was fitted with a double gap concentric cylinder with inside and outside cup diameters of 27.732 mm and 33.995 mm, respectively, and inside and outside bob diameters of 29.396 mm and 32.080 mm, respectively. The geometry features rectangular windows at the top of the bob and the bottom of the cup, the former allows the free surface of the sample to sit within the window hence minimising surface tension effects during orthogonal experiments. The latter allows sample to move freely between the 'measurement annulus' and a sample reservoir which sits within the inner cup; in this manner, pumping flows are minimised and a uniform velocity gradient is achieved during orthogonal superposition experiments [11,31]. The submersed height of the bob was 43.6 mm with an operating gap of 8 mm. Prior to measurements being performed, geometry end-effect correction factors were calibrated using a 970 mPa s Newtonian Silicone Oil (Brookfield). Measurements were performed at 20 °C with temperature control being achieved via the TA Instruments Advanced Peltier System. A thin layer of silicone oil was added to the free surface of the sample (positioned in the centre of the bob windows) to prevent solvent evaporation during measurement. The sample was loaded and conditioned (at rest) for 900 s at the desired temperature before being pre-sheared at 1 s^{-1} for 60 s. The sample was then allowed to rest for a further 60 s before rheological measurements were performed.

Rheological characterisation involved (i) determination of the linear viscoelastic range (LVR) using a strain sweep, (ii) acquisition of frequency sweep data $0.64\ \text{rad/s} \le \omega \le 100\ \text{rad/s}$ at a strain amplitude within the LVR, (ii) acquisition of a steady state flow sweep which was performed in the reverse direction (100 s^{-1} to 0.1 s^{-1}) (iii) identification of the 'parallel superposition linear range' (PS-LVR) using oscillatory strain sweeps at each unidirectional shear rate (iv) acquisition of parallel superposition frequency sweep data at the strain amplitude within the PS-LVR, (v) identification of the OS-LVR for orthogonal superposition measurements using orthogonal strain sweeps (for which the strain range is limited by a maximum axial displacement of 50 μm), and (vi) acquisition of orthogonal superposition frequency sweep data at a strain amplitude within the OS-LVR. All experiments were undertaken in triplicate with data processing being undertaken on the averaged data.

Rheometric slip artefacts (i.e. local velocity gradients close to the geometry walls — distinct from the 'slip' of the GS/JS models) are difficult to assess in the concentric cylinder geometries necessary for performing orthogonal superposition experiments. However, we have recently used the same WLM formulation in a study of start-up shear flows in which no evidence of rheometric slip was observed [32].

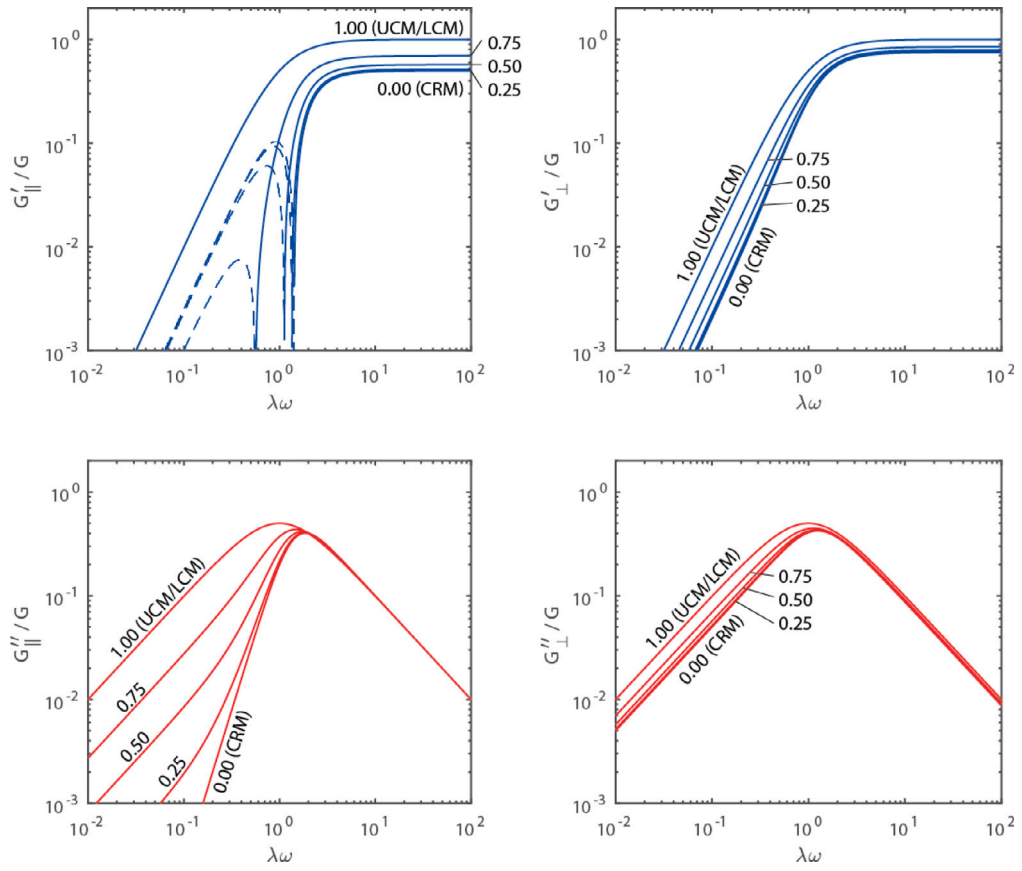

Fig. 1. Superposition moduli as a function of Deborah number for $Wi = 1.0$ for a single mode GS model for $a = 0.00$ (CRM), $|a| = 0.25, 0.5, 0.75$ and $|a| = 1.00$ (UCM for $a = 1.00$ and LCM for $a = -1.00$).

3.3. Data processing

Data was processed using two fitting algorithms. The first (procedure A) assumed a weakly nonlinear response in that the underlying linear viscoelastic spectrum was not permitted to be a function of shear rate, the second (procedure B) allowed the underlying viscoelastic spectrum to be rate dependent thus permitting strongly-nonlinear behaviour [18].

3.3.1. Data analysis procedure A: Weakly non-linear

To parameterise the weakly non-linear CRJ model, linear viscoelastic data ($G'(\omega)$, $G''(\omega)$) and viscometry data were fitted to a single mode CRM model with a Newtonian solvent thus involving 3 parameters ($[\lambda_1, \eta_0, \eta_1]$). Similarly, to parameterise the GS model, linear viscoelastic data ($G'(\omega)$, $G''(\omega)$) and the viscometry data were fitted to a single-mode GS model with a Newtonian solvent and the expression for the viscosity of the GS model, namely,

$$\eta(\dot{\gamma}) = \frac{\eta_0}{1 + \lambda_1^2\dot{\gamma}^2(1 - a^2)} + \eta_1 \tag{3.1}$$

Thus the parameterisation of the GS model involved 4 parameters ($[\lambda_1, \eta_0, \eta_1, a]$).

The parameterised models were then used to predict the parallel and orthogonal data ($G'_{\parallel}$, $G''_{\parallel}$ and $G'_{\perp}$, $G''_{\perp}$, respectively) for the CRJ ($a = 0$) and GS models.

3.3.2. Data analysis procedure B: Strongly non-linear

Analysis procedure B involved treating the data such that each shear rate defined a discrete and independent material state. Parallel and orthogonal moduli were simultaneously fitted at each shear rate. This approach admitted the possibility of shear-induced modification of the underlying relaxation spectrum thus allowing strong non-linearity [18].

4. Results & discussion

4.1. Weakly non-linear analysis

We begin by evaluating the CRJ model's ability to describe the dynamics of the WLM system using a weakly non-linear analysis. Fig. 2A and B show the SAOS and viscometry data for the sample, respectively. The parameters of the model were determined from the SAOS data and viscometry data. The lines on Fig. 2A and B show the best fit to this data as determined using a nonlinear least squares routine which minimised the RMS relative errors between the experimental data (SAOS and $\eta(\dot{\gamma})$) and the model [$\lambda_1 = 0.49$ s, $\eta_0 = 26.63$ Pa s, $\eta_1 = 0.06$ Pa s]. Having parameterised the CRJ model, the real parts of the superposition moduli (in both parallel and orthogonal configurations, $G'_{\parallel}(\omega, \dot{\gamma})$ and $G'_{\perp}(\omega, \dot{\gamma})$) were evaluated using Eqs. (2.38) and (2.49) with $a = 0$. Whilst the imaginary parts required the addition of the solvent viscosity (η_1) term and hence were calculated using Eqs. (2.53) and (2.54).

Fig. 2C through G show experimental data and the parameterised CRJ model over a range of shear rates for the PSR experiment whilst Fig. 2H through L show equivalent data for the OSR experiment. At low rates, $\dot{\gamma} < 1$ s^{-1}, the model and experimental data are in good agreement. However, as the shear rate increases $\dot{\gamma} \geq 1$ s^{-1}, the weakly non-linear analysis based on the CRJ model does not describe the data with significant discrepancies appearing in (i) both the real and imaginary parts of the superposition moduli and, (ii) the viscosity data of Fig. 2B. The CRJ model is known to excessively shear thin where the ratio $\eta_1/\eta_0 < 1/3$ [33]. This ratio evaluates as $\approx$0.02 for the current parameterisation and hence the criterion for realistic shear thinning is clearly not met. It is hence unsurprising that the CRJ model fails in terms of predicting the superposition moduli at high rates.

We hence conclude that, for the specific WLM system studied herein, a weakly non-linear analysis of the superposition moduli based on the

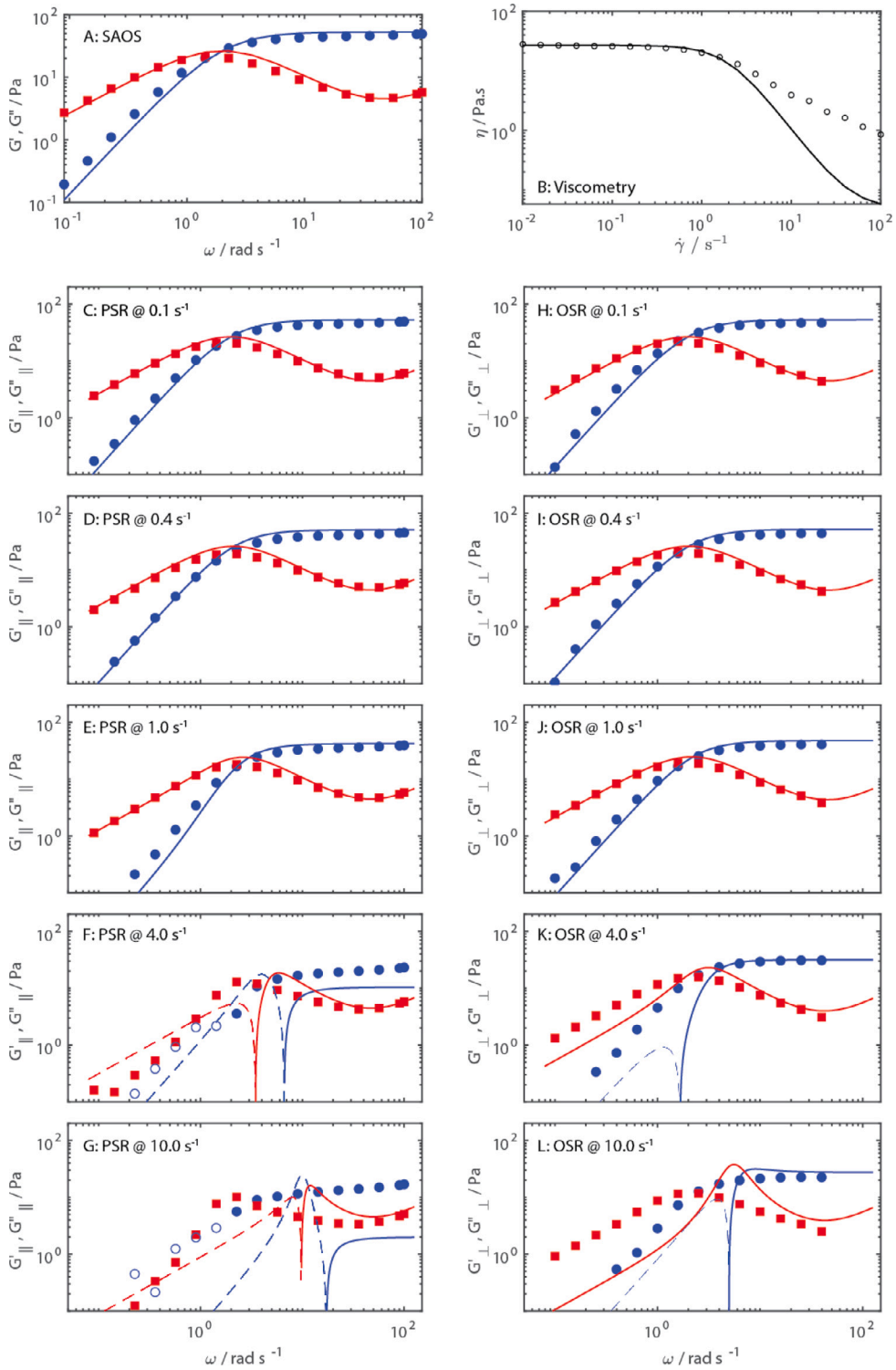

Fig. 2. Weakly non-linear analysis (analysis A) for the corotational Jeffrey's Model. Real and imaginary parts of the complex moduli are shown as blue circles and red squares, respectively, with open symbols referring to negative moduli. Lines correspond to the CRJ model with dashed lines indicating negative moduli.

CRJ model does not capture the appropriate dynamics of the system at $\dot{\gamma} > 1\ s^{-1}$. A recent paper by Lennon et al. [25] employing the MAPS protocol (Medium Amplitude Parallel Superposition) concluded that the CRJ model was able to capture the weakly non-linear behaviour of an almost identical WLM formulation. It is important to note, however, that the MAPS protocol employed in [25] used oscillatory flows, at a number of frequencies simultaneously, with no steady flow component, whilst in the PSR/OSR protocols employed herein, the material is subjected to a sustained unidirectional flow. The two results are hence not in direct conflict.

The parameter a in the GS/JS model serves to modify the shear-thinning characteristics of the CRJ model. Increasing a shifts the shear thinning region to higher $\dot{\gamma}$ with the limit $a = 1$ shifting it to infinitely high rates such that shear thinning does not occur. We now evaluate the ability of GS/JS model (using a weakly non-linear analysis) to capture the dynamics of the WLM sample under superposition flows. As for the

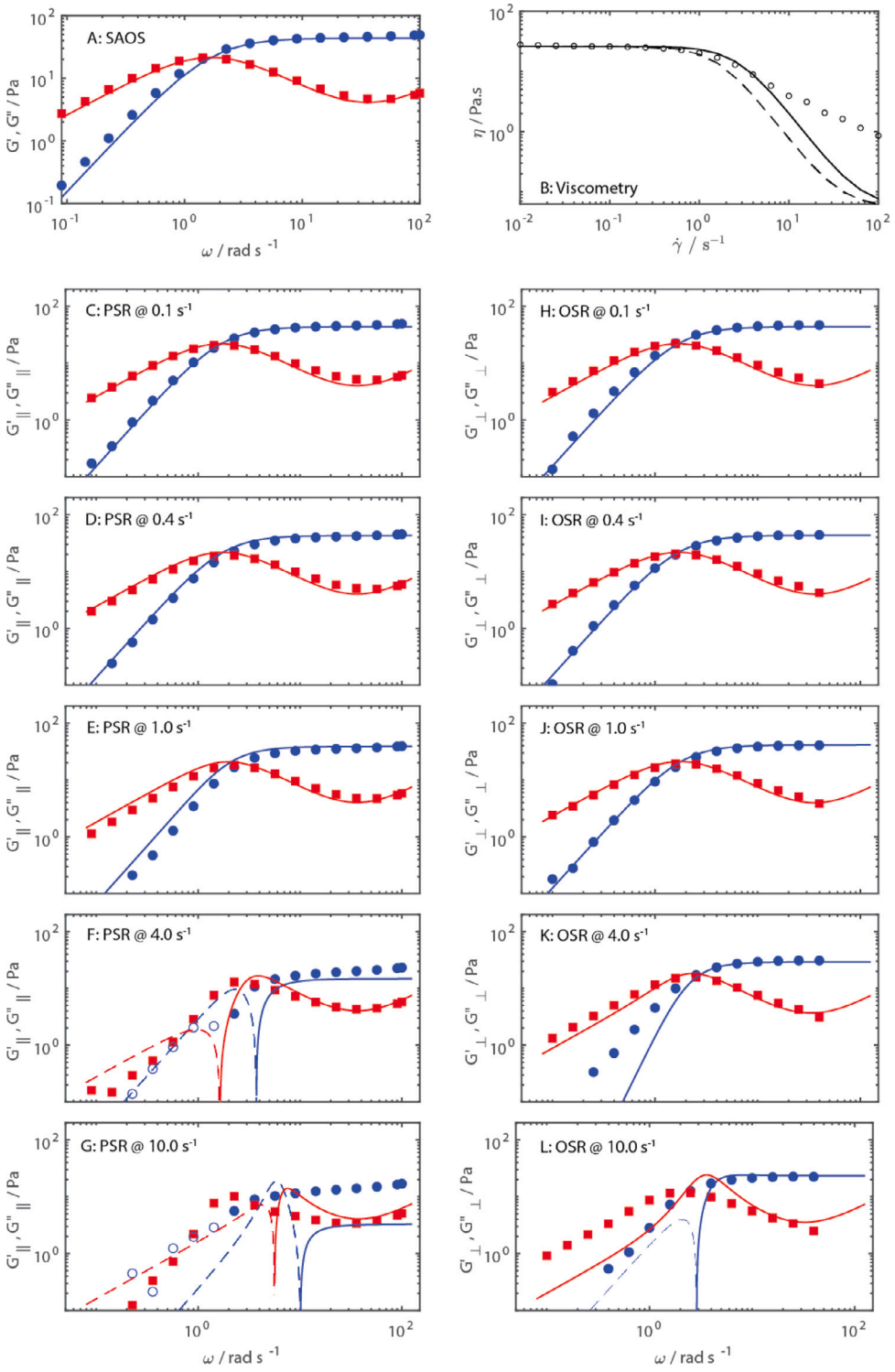

Fig. 3. Weakly non-linear analysis (analysis A) for the Gordon–Schowalter Model. Real and imaginary parts of the complex moduli are shown as blue circles and red squares, respectively, with open symbols referring to negative moduli. Lines correspond to the GS model with dashed lines indicating negative moduli. In sub figure B, the CRJ model is also shown (as a dashed line) for reference.

CRM model, we parameterise the model based on SAOS and viscometry data (see fits shown in Fig. 3A and B) before comparing the model's superposition moduli with the experimental data. It is notable that significant deviation is still observed in both the superposition data at $\dot{\gamma} > 1$ s^{-1} and the viscometry data for $\dot{\gamma} > 4$ s^{-1} indicating, as for the CRJ model, that a weakly nonlinear application of the GS model is insufficient to capture the dynamics of the specific WLM system studied herein under superposition flows.

4.2. Strongly non-linear analysis

In Section 4.1 the CRJ and GS models were parameterised based on SAOS and viscometry data alone. Consequently, the superposition moduli may considered to be predictions to which experimental data can be compared in order to evaluate the model's validity for the fluid being studied. In this respect, both the CRJ and GS models were unsuitable for the specific worm-like micellular system being investigated

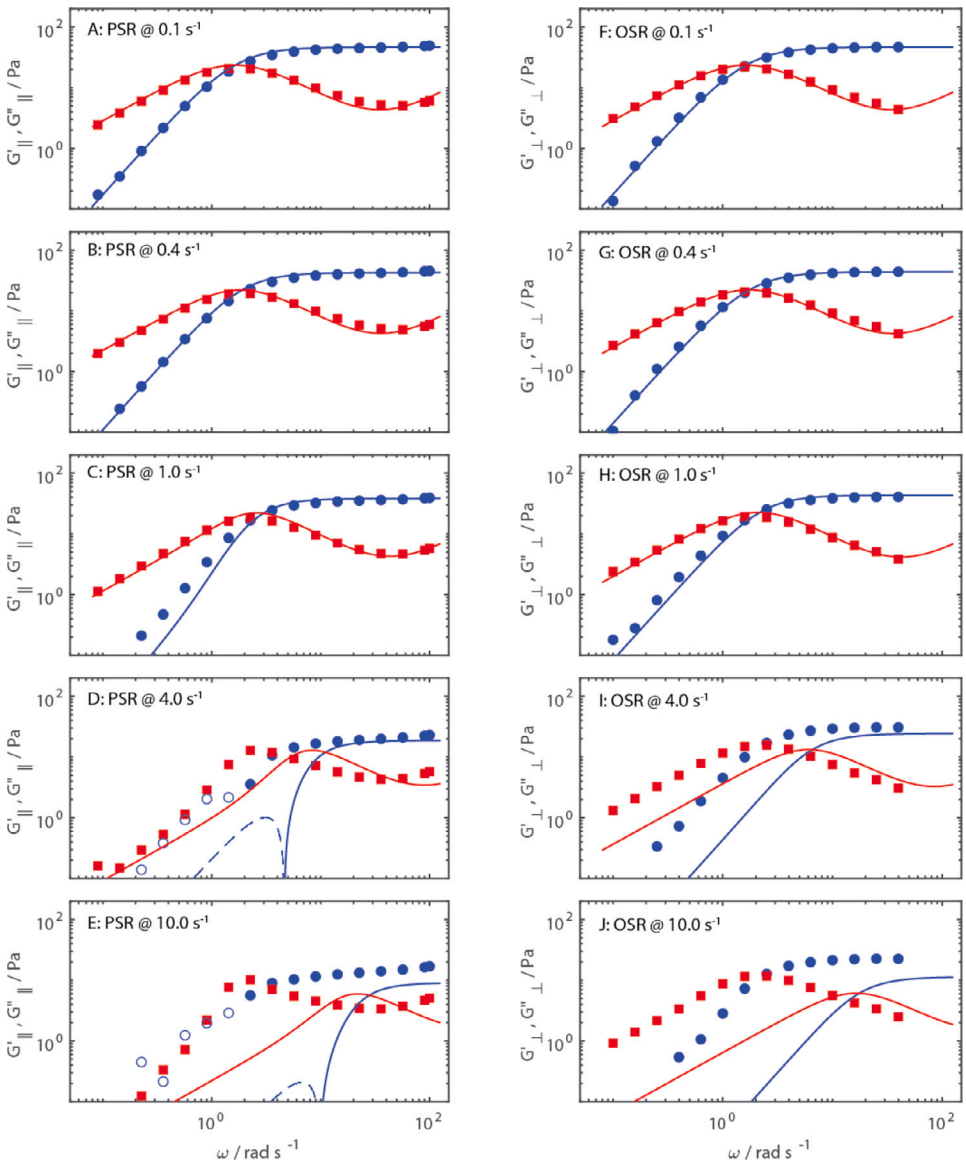

Fig. 4. Strongly non-linear analysis (analysis B) for the Corotational Jeffreys Model. Real and imaginary parts of the complex moduli are shown as blue circles and red squares, respectively, with open symbols referring to negative moduli. Lines correspond to the CRJ model with dashed lines indicating negative moduli.

at shear rates for which shear thinning is observed. In this section, we relax the requirement for the underlying relaxation characteristics of the material to be independent of shear-rate, treating each shear rate as defining an independent material state characterised by its parallel and orthogonal moduli. This approach permits strong non-linearity in which rate-dependent model parameters indicate microstructural modification by the imposed flow conditions.

Fig. 4 shows the results of this 'strongly non-linear analysis' (referred to as analysis B in Section 3.3.2) for the CRJ model. The fitting procedure was unable to determine model parameters that satisfied the data at rates higher than 1 s^{-1} indicating that, even by permitting strong non-linearity into the analysis, the CRJ is unsuitable for this specific formulation. Undertaking a similar analysis based on the GS/JS model generates significantly better agreement between the experimental data and the GS/JS model as shown in Fig. 5. Even at the highest shear rate studied ($\dot{\gamma} = 10$ s^{-1}) the strongly non-linear GS/JS model is able to capture both sets of superposition moduli very well.

Fig. 7 and Table 1 show the GS model parameters as a function of shear rate. Interestingly, a, which is often interpreted as a 'slip' parameter increases with shear rate (for $\dot{\gamma} > 0.4$ s^{-1}) such that the system appears to transition from the CRJ model ($a = 0$) towards the Oldroyd-B model ($a = 1$). In both Fig. 7C and Table 1, the value of a at 0.1 s^{-1} has been fixed at 0.0 since the data closely resembles the SAOS data and hence the parameter has negligible effect. Interestingly, the relaxation time, λ_1 (Fig. 7A) appears to be largely insensitive to the shear rate whilst η_0 begins to decrease significantly for $\dot{\gamma} > 1$ s^{-1}. This suggests that changes in the superposition moduli for the specific WLM system studied herein, are driven predominantly by a change in deformation type rather than a change in microstructure (though a shear-sensitive η_0 would suggest microstructural changes remain important).

In a recent publication, Ramlawi et al. [17] considered the weakly nonlinear response of the GS/JS model in terms of a Medium Amplitude Oscillatory Shear (MAOS) experiment. As part of their contribution, they provided a framework for visualising the non-affine deformation of GS/JS type models in terms of the deformation of a Lagrangian element. Following this approach, Fig. 6 compares the deformation patterns for $a = 0$, i.e. pure rotation, $a = 0.5$ and $a = 1.0$, i.e. different combinations of stretching and rotation. The deformation rate of the bulk solvent is shown as a dashed line.

The data suggest that as the imposed shear rate increases, the microstructural elements of the fluid undergo deformation involving an

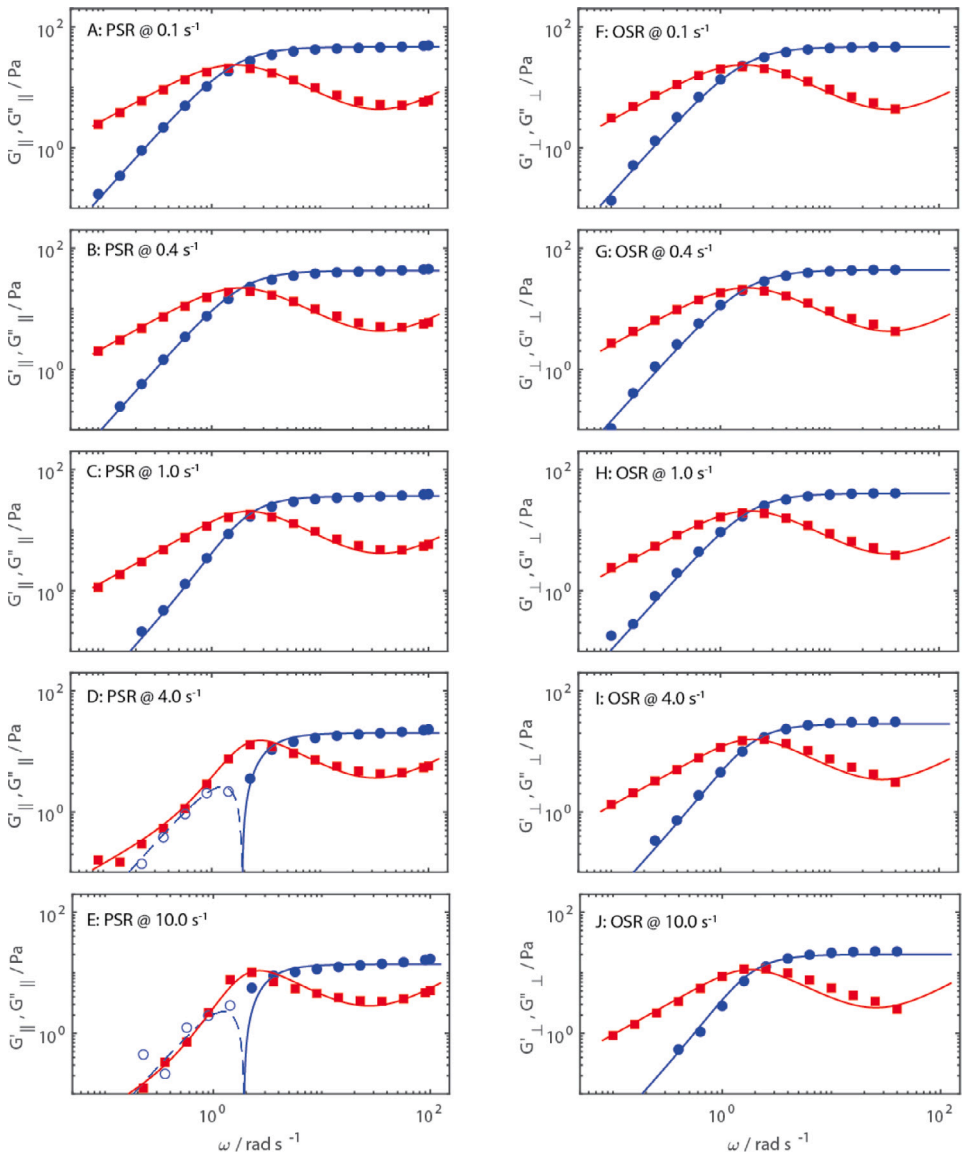

Fig. 5. Strongly non-linear analysis (analysis B) for the Gordon–Schowalter Model. Real and imaginary parts of the complex moduli are shown as blue circles and red squares, respectively, with open symbols referring to negative moduli. Lines correspond to the GS model with dashed lines indicating negative moduli.

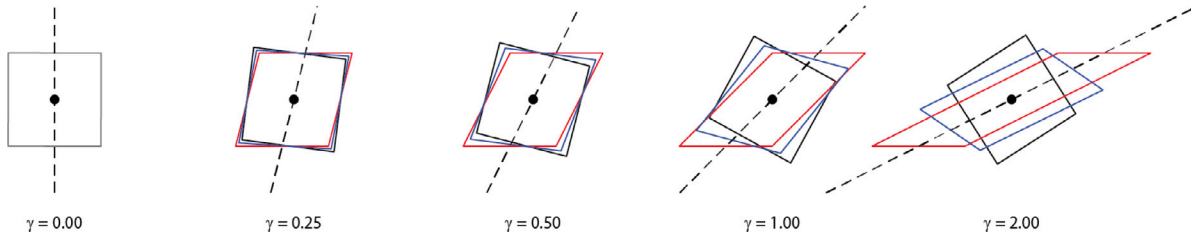

Fig. 6. Visualisation of the nonaffine deformation for $a = 0$ (black), $a = 0.5$ (blue) and $a = 1$ (red) at accumulated strains of $0 \leq \gamma \leq 2$. The dashed line corresponds to the accumulated strain of the bulk deformation/solvent.

increasing degree of stretching, which disrupts the micellular network, thus resulting in a decreased viscosity.

Whilst the superposition moduli can be described well by a strongly non-linear GS/JS analysis, the model parameters at each shear rate do not generate the correct value of the viscosity. Fig. 8 shows the experimental viscosity data (open symbols) and the viscosity as calculated from the model parameters at each of the 5 shear rates for which superposition moduli are available. The model and the experimental data agree at low rates ($\dot{\gamma} \leq 1.0\ s^{-1}$) but the model fails increasingly as the shear rate increases above $1.0\ s^{-1}$ suggesting that the model does not capture the required physics.

5. Conclusions

In the present work, expressions for the superposition moduli for the Gordon–Schowalter/Johnson–Segalman model have been derived for the first time. Included, as special cases, within the GS/JS model are the corotational Maxwell Model (which was considered by Curtis & Davies

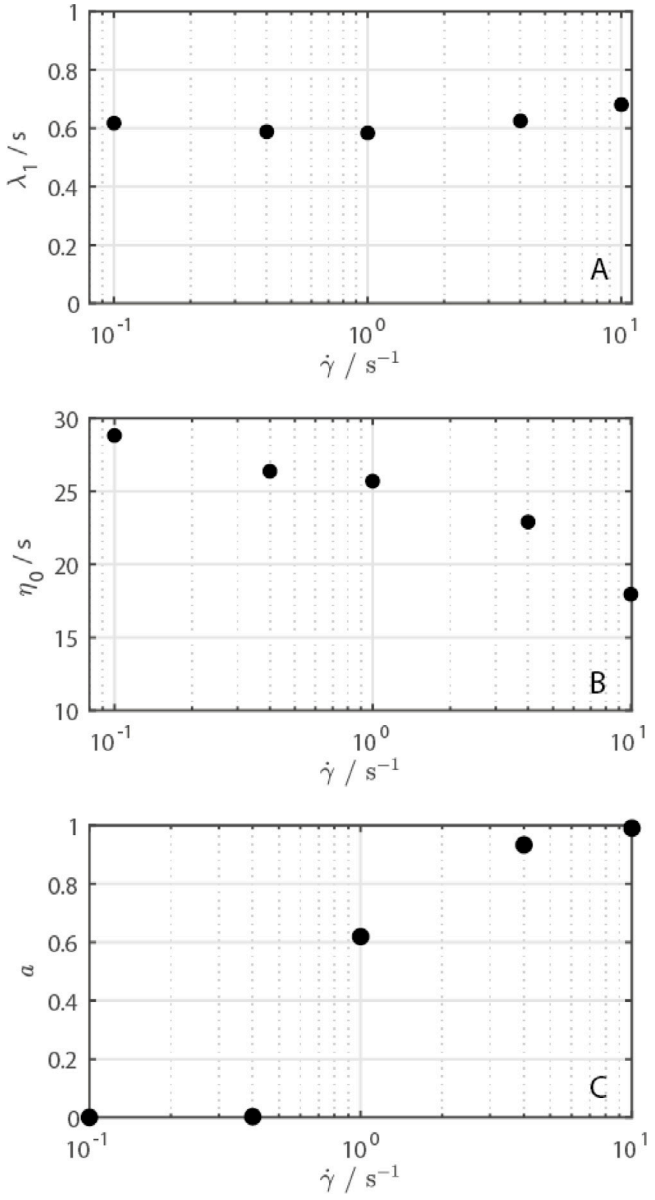

Fig. 7. Variation of GS model parameters as a function of shear rate.

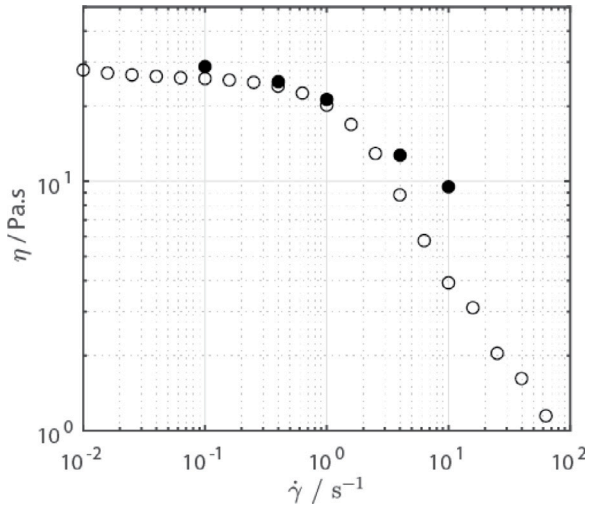

Fig. 8. Viscosity as calculated from strongly non-linear JS parameters.

Table 1
JS parameters.

$\dot{\gamma}$ (s^{-1})	λ_1 (s)	η_0 (Pa s)	η_1 (Pa s)	a (–)
0.1	0.62	28.8	0.06	0.0000[a]
0.4	0.59	26.4	0.06	0.0024
1.0	0.58	25.7	0.06	0.6189
4.0	0.62	22.9	0.06	0.9328
10.0	0.68	18.0	0.05	0.9902

[a] At very low rates, the expressions for the superposition moduli are insensitive to the value of 'a' hence, in the table above its value has been fixed at $a = 0.0$.

in [5], the upper and lower convected Maxwell models, and, with the addition a Newtonian solvent contribution, the corotational Jeffreys model and the Oldroyd-B fluid (the superposition moduli of which were first considered by Booij in 1966 [24]). It is also conjectured that shear thinning is necessary, but not sufficient, for the appearance of negative superposition moduli. Further, the ability of the GS/JS model (and its associated special cases) to describe the superposition moduli of a specific Worm Like Micellular system has been evaluated using (i) weakly and (ii) strongly non-linear analyses. The weakly non-linear analysis (in which the model parameters have been determined based on the linear viscoelastic and viscometry data alone) was found to be unable to describe the superposition moduli at shear rates beyond the onset of shear thinning. However, by permitting the model parameters to become shear rate dependent, thus admitting strong non-linearity (in the context of Malkin's classifications [18]), the GS/JS model was found to fit the superposition moduli at all rates extremely well. The shear rate-dependent GS/JS parameters suggest that the onset of shear thinning in the specific WLM system studied herein is associated with a gradual change in the deformation experienced by the microstructural elements of the fluid, the stretching element of the deformation becoming increasingly important as $\dot{\gamma}$ increases.

CRediT authorship contribution statement

A. Ogunkeye: Writing – original draft, Investigation. **R. Hudson-Kershaw:** Writing – original draft, Investigation. **A.R. Davies:** Writing – review & editing, Validation, Investigation, Conceptualization. **D.J. Curtis:** Writing – review & editing, Writing – original draft, Validation, Supervision, Investigation, Conceptualization.

Declaration of competing interest

The authors declare the following financial interests/personal relationships which may be considered as potential competing interests: Daniel Jonathan Curtis reports financial support was provided by Engineering and Physical Sciences Research Council. Daniel Jonathan Curtis reports financial support was provided by Welsh Government. A. Russell Davies reports financial support was provided by Engineering and Physical Sciences Research Council. Daniel J. Curtis is serving as a Guest Editor for the Special Issue of JNNFM to which this article is being submitted (DC). The journal's Editors-in-Chief will process and make decisions regarding the manuscript. If there are other authors, they declare that they have no known competing financial interests or personal relationships that could have appeared to influence the work reported in this paper.

Data availability

Data will be made available on request.

Acknowledgements

DJC & REH acknowledge the support of EPSRC, UK through grant EP/T026154/1. DJC also acknowledges financial support from EPSRC, UK through grant EP/N013506/1 & and the European Regional Development Fund via Llywodraeth Cymru (AFM^2 and IMPACT Projects). ARD acknowledges the support of EPSRC, UK through the Inverse Problems Network grant EP/P005985/1. All authors would like to thank Mr Mark Ellis & Mr Ray Williams, both of TA Instruments, for their support in upgrading the ARES-G2 used in this study to perform Orthogonal Superposition Experiments and Prof. Jan Vermant for his advice regarding orthogonal superposition experiments.

Appendix. Expansion of the stress tensor about the viscometric case for orthogonal superposition

Noting that the stress tensor is symmetrical we can write the following system of 6 simultaneous linear differential equations:

$$\tau_{11} + \lambda\dot{\tau}_{11} - \lambda_1\tau_{12}\dot{\gamma}(1+a) = 0$$

$$\tau_{12} + \lambda_1\dot{\tau}_{12} - \frac{\lambda_1}{2}\left[\tau_{22}\dot{\gamma}(1+a) + \tau_{11}\dot{\gamma}(a-1) + \tau_{13}\epsilon\dot{\phi}(a-1)\right] = \dot{\gamma}\eta_0$$

$$\tau_{13} + \lambda_1\dot{\tau}_{13} - \frac{\lambda_1}{2}(1+a)[\tau_{23}\dot{\gamma} + \tau_{12}\epsilon\dot{\phi}] = 0$$

$$\tau_{22} + \lambda_1\dot{\tau}_{22} + \lambda_1\left[(1-a)\tau_{12}\dot{\gamma} + (1-a)\tau_{32}\epsilon\dot{\phi}\right] = 0$$

$$\tau_{23} + \lambda_1\dot{\tau}_{23} + \frac{\lambda_1}{2}(1-a)\tau_{13}\dot{\gamma} + \frac{\lambda_1}{2}(1-a)\tau_{33}\epsilon\dot{\phi} - \frac{\lambda_1}{2}\tau_{22}\epsilon\dot{\phi}(1+a) = \epsilon\dot{\phi}\eta_0$$

$$\tau_{33} + \lambda_1\dot{\tau}_{33} = 0$$

Setting $\epsilon = 0$ we obtain the 'viscometric case'...

$$\tau_{11}^{(0)} = \frac{\eta_0\lambda_1\dot{\gamma}^2(1+a)}{1+\lambda_1^2\dot{\gamma}^2(1-a^2)}$$

$$\tau_{22}^{(0)} = -\frac{\eta_0\lambda_1\dot{\gamma}^2(1-a)}{1+\lambda_1^2\dot{\gamma}^2(1-a^2)}$$

$$\tau_{12}^{(0)} = \frac{\eta_0\dot{\gamma}}{1+\lambda_1^2\dot{\gamma}^2(1-a^2)}$$

with $\tau_{13} = \tau_{23} = \tau_{33} = 0$. We now expand about the viscometric case using (2.26) such that, to first order in ϵ:

$$\tau_{11}^{(0)} + \epsilon\tau_{11}^{(1)} + \lambda\epsilon\dot{\tau}_{11}^{(1)} - \lambda_1\tau_{12}^{(0)}\dot{\gamma}(1+a) - \lambda_1\epsilon\tau_{12}^{(1)}\dot{\gamma}(1+a) = 0$$

$$\tau_{12}^{(0)} + \epsilon\tau_{12}^{(1)} + \lambda_1\epsilon\dot{\tau}_{12}^{(1)} - \frac{\lambda_1}{2}\left[\tau_{22}^{(0)}\dot{\gamma}(1+a) + \epsilon\tau_{22}^{(1)}\dot{\gamma}(1+a) + \tau_{11}^{(0)}\dot{\gamma}(a-1) + \epsilon\tau_{11}^{(1)}\dot{\gamma}(a-1) + \tau_{13}^{(0)}\epsilon\dot{\phi}(a-1)\right] = \dot{\gamma}\eta_0$$

$$\tau_{13}^{(0)} + \epsilon\tau_{13}^{(1)} + \epsilon\lambda_1\dot{\tau}_{13}^{(1)} - \frac{\lambda_1}{2}(1+a)[\tau_{23}^{(0)}\dot{\gamma} + \epsilon\tau_{23}^{(1)}\dot{\gamma} + \tau_{12}^{(0)}\epsilon\dot{\phi}] = 0$$

$$\tau_{22}^{(0)} + \epsilon\tau_{22}^{(1)} + \lambda_1\epsilon\dot{\tau}_{22}^{(1)} + \lambda_1\left[(1-a)\tau_{12}^{(0)}\dot{\gamma} + \epsilon(1-a)\tau_{12}^{(1)}\dot{\gamma} + (1-a)\tau_{32}^{(0)}\epsilon\dot{\phi}\right] = 0$$

$$\tau_{23}^{(0)} + \epsilon\tau_{23}^{(1)} + \lambda_1\epsilon\dot{\tau}_{23}^{(1)} + \frac{\lambda_1}{2}(1-a)\tau_{13}^{(0)}\dot{\gamma} + \frac{\lambda_1}{2}(1-a)\epsilon\tau_{13}^{(1)}\dot{\gamma} + \frac{\lambda_1}{2}(1-a)\tau_{33}^{(0)}\epsilon\dot{\phi} - \frac{\lambda_1}{2}\tau_{22}^{(0)}\epsilon\dot{\phi}(1+a) = \epsilon\dot{\phi}\eta_0$$

$$\tau_{33}^{(0)} + \epsilon\tau_{33}^{(1)} + \lambda_1\epsilon\dot{\tau}_{33}^{(1)} = 0$$

Substituting the expressions for the viscometric case and recalling earlier definitions of α and β,

$$\alpha = \frac{\eta_0\lambda_1\dot{\gamma}(1+a)}{1+\lambda_1^2\dot{\gamma}^2(1-a^2)}$$

$$\beta = \frac{\eta_0}{1+\lambda_1^2\dot{\gamma}^2(1-a^2)}$$

we can write:

$$\tau_{11}^{(1)} + \lambda\dot{\tau}_{11}^{(1)} - \lambda_1\tau_{12}^{(1)}\dot{\gamma}(1+a) = 0$$

$$\epsilon\tau_{12}^{(1)} + \lambda_1\epsilon\dot{\tau}_{12}^{(1)} - \frac{\lambda_1}{2}\left[\epsilon\tau_{22}^{(1)}\dot{\gamma}(1+a) + \epsilon\tau_{11}^{(1)}\dot{\gamma}(a-1)\right] = \dot{\gamma}\eta_0 - \beta\dot{\gamma}$$

$$\tau_{13}^{(1)} + \lambda_1\dot{\tau}_{13}^{(1)} - \frac{1}{2}\lambda_1\dot{\gamma}(1+a)\tau_{23}^{(1)} = \frac{1}{2}\alpha\dot{\phi}$$

$$\tau_{22}^{(1)} + \lambda_1\dot{\tau}_{22}^{(1)} + \lambda_1\dot{\gamma}(1-a)\tau_{12}^{(1)} = 0$$

$$\tau_{23}^{(1)} + \lambda_1\dot{\tau}_{23}^{(1)} + \frac{\lambda_1}{2}(1-a)\tau_{13}^{(1)}\dot{\gamma} = \frac{1}{2}(\beta+\eta_0)\dot{\phi}$$

$$\epsilon\tau_{33}^{(1)} + \lambda_1\epsilon\dot{\tau}_{33}^{(1)} = 0$$

The equations above involving orthogonal components (i.e τ_{13}) form a pair of linear differential equations:

$$\tau_{13}^{(1)} + \lambda_1\dot{\tau}_{13}^{(1)} - \frac{1}{2}\lambda_1\dot{\gamma}(1+a)\tau_{23}^{(1)} = \frac{1}{2}\alpha\dot{\phi}$$

$$\tau_{23}^{(1)} + \lambda_1\dot{\tau}_{23}^{(1)} + \frac{\lambda_1}{2}\dot{\gamma}(1-a)\tau_{13}^{(1)} = \frac{1}{2}(\beta+\eta_0)\dot{\phi}$$

which appear in the main manuscript.

References

[1] M. Yamamoto, Rate-dependent relaxation spectra and thier determination, Trans. Soc. Rheol. 15 (1971) 331–344.
[2] S. Kim, J. Mewis, C. Clasen, J. Vermant, Superposition rheometry of a wormlike micellar fluid, Rheol. Acta 52 (2013) 727–740.
[3] D.J. Curtis, A.R. Davies, On shear-rate dependent relaxation spectra in superposition rheometry: A basis for quantitative comparison/interconversion of orthogonal and parallel superposition moduli, J. Non-Newton. Fluid Mech. 274 (2019) 104198.
[4] D.J. Curtis, A.R. Davies, On response spectra and Kramers-Kronig relations in superposition rheometry, Phys. Fluids 31 (12) (2019) 127105.
[5] D.J. Curtis, A.R. Davies, Volterra kernels, Oldroyd models, and interconversion in superposition rheometry, J. Non-Newton. Fluid Mech. 293 (2021) 104554.
[6] K. Osaki, Complex modulus of concentrated polymer solutions in steady shear, J. Phys. Chem. 69 (1965) 4183–4191.
[7] H. Booij, Influence of superimposed steady shear flow on the dynamic properties on non-Newtonian fluids I: Measurements on non-Newtonian solutions, Rheol. Acta 5 (1966) 215–221.
[8] A. Lodge, Elastic Liquids, first ed., Academic Press, London, 1964.
[9] I.F. Macdonald, R.B. Bird, Complex modulus of concentrated polymer solutions in steady shear, J. Phys. Chem. 70 (1966) 2068–2069.
[10] G. Colombo, K Sunhyung, T. Schweizer, B Schroyen, C Clasen, J Mewis, J Vermant, Superposition rheology and anisotropy in rheological properties of sheared colloidal gels, J. Rheol. 61 (2017) 1035–1048.
[11] J. Vermant, P. Moldenaers, J. Mewis, M Ellis, R. Garritano, Orthogonal superposition measurements using a rheometer equipped with a force rebalanced transducer, Rev. Sci. Instrum. 68 (1997) 4090.
[12] J. Vermant, L. Walker, P. Moldenaers, J. Mewis, Orthogonal versus parallel superposition measurements, J. Non-Newton. Fluid Mech. 79 (1998) 173–189.
[13] J. Simmons, A servo-controlled rheometer for measurement of the dynamic modulus of viscoelastic liquids, Sci. Instrum. 43 (1966) 887.
[14] Jos Zeegers, Dirk van den Ende, Cor Blom, Egbert G. Altena, Gerrit J. Beukema, Jorrit Mellema, A sensitive dynamic viscometer for measuring the complex shear modulus in a steady shear flow using the method of orthogonal superposition, Rheol. Acta 34 (6) (1995) 606–621.
[15] R.J. Gordon, W.R. Schowalter, Anisotropic fluid theory: A different approach to the dumbbell theory of dilute polymer solutions, Trans. Soc. Rheol. 16 (1) (1972).
[16] M.W. Johnson, D. Segalman, A model for viscoelastic fluid behavior which allows non-affine deformation, J. Non-Newton. Fluid Mech. 2 (3) (1977).
[17] N. Ramlawi, N.A. Bharadwaj, R.H. Ewoldt, The weakly nonlinear response and nonaffine interpretation of the Johnson–Segalman/Gordon–Schowalter model, J. Rheol. 64 (2020) 1409.
[18] A.Y. Malkin, Non-linearity in rheolgoy - as essay of classification, Rheol. Acta 34 (1995) 27–39.
[19] V.J. Anderson, J.R. Am Perason, E. Boek, The rheology of wormlike micellar fluids, Rheol. Rev. 2006 (The British Society of Rheology) (2006).

[20] M.E. Cates, Nonlinear viscoelasticity of wormlike micelles (and other reversibly breakable polymers), J. Phys. Chem. 94 (1) (1990) 371–375.
[21] B. Yesilata, C. Clasen, G.H. McKinley, Nonlinear shear and extensional flow dynamics of wormlike surfactant solutions, J. Non-Newton. Fluid Mech. 133 (2) (2006) 73–90.
[22] V.J. Anderson, J.R.A. Pearson, J.D. Sherwood, Oscillation superimposed on steady shearing: Measurements and predictions for wormlike micellar solutions, J. Rheol. 50 (2006) 771–796.
[23] Pierre Ballesta, M. Paul Lettinga, Sébastien Manneville, Superposition rheology of shear-banding wormlike micelles, J. Rheol. 51 (5) (2007) 1047–1072.
[24] H. Booij, Influence of superimposed steady shear flow on the dynamic properties of non-Newtonian fluids. II. Theoretical approach based on the oldroyd theory, Rheol. Acta 5 (1966) 222–227.
[25] Kyle R. Lennon, Michela Geri, Gareth H. McKinley, James W. Swan, Medium amplitude parallel superposition (MAPS) rheology. Part 2: Experimental protocols and data analysis, J. Rheol. 64 (5) (2020) 1263–1293.
[26] P.D. Olmsted, O. Radulescu, C.-Y.D. Lu, Johnson–Segalman model with a diffusion term in cylindrical Couette flow, J. Rheol. 44 (2) (2000) 257–275.
[27] Helen J. Wilson, Suzanne M. Fielding, Linear instability of planar shear banded flow of both diffusive and non-diffusive johnson–segalman fluids, J. Non-Newton. Fluid Mech. 138 (2) (2006) 181–196.
[28] Y.T. Hu, A. Lips, Kinetics and mechanism of shear banding in an entangled micellar solution, J. Rheol. 49 (2005) 1001–1047.
[29] Y.T. Hu, C. Palla, A. Lips, Comparison between shear banding and shear thinning in entangled micellar solutions, J. Rheol. 52 (2008) 379–400.
[30] P. Cheng, M.C. Burroughs, G.L. Leal, M.E. Helgeson, Distinguishing shear banding from shear thinning in flows with a shear stress gradient, Rheol. Acta 56 (2017) 1007–1032.
[31] R. Tao, A.M Forster, End effect correction for orthogonal small strain oscillatory shear in a rotational shear rheometer, Rheol. Acta 59 (2020) 95–108.
[32] A. Ogunkeye, R.E. Hudson, D.J. Curtis, The effect of instrument inertia on the initiation of oscillatory flow in stress controlled rheometry, J. Rheol. 67 (6) (2023) 1175–1187.
[33] R. Bird, R. Armstrong, O. Hassager, Dynamics of Polymeric Liquids, John Wiley & Sons, New York, 1977.